

Detection of brown adipose tissue and thermogenic activity in mice by hyperpolarized xenon MRI

Rosa Tamara Branca^{a,b,1}, Ting He^c, Le Zhang^{a,b}, Carlos S. Floyd^a, Matthew Freeman^d, Christian White^a, and Alex Burant^{a,b}

^aDepartment of Physics and Astronomy, ^bBiomedical Research Imaging Center, and ^cDepartment of Pharmacology, University of North Carolina at Chapel Hill, Chapel Hill, NC 27599; and ^dMedical Physics Graduate Program, Duke University, Durham, NC 27708

Edited* by William Happer, Princeton University, Princeton, NJ, and approved October 30, 2014 (received for review February 27, 2014)

The study of brown adipose tissue (BAT) in human weight regulation has been constrained by the lack of a noninvasive tool for measuring this tissue and its function *in vivo*. Existing imaging modalities are nonspecific and intrinsically insensitive to the less active, lipid-rich BAT of obese subjects, the target population for BAT studies. We demonstrate noninvasive imaging of BAT in mice by hyperpolarized xenon gas MRI. We detect a greater than 15-fold increase in xenon uptake by BAT during stimulation of BAT thermogenesis, which enables us to acquire background-free maps of the tissue in both lean and obese mouse phenotypes. We also demonstrate *in vivo* MR thermometry of BAT by hyperpolarized xenon gas. Finally, we use the linear temperature dependence of the chemical shift of xenon dissolved in adipose tissue to directly measure BAT temperature and to track thermogenic activity *in vivo*.

MRI | hyperpolarized ¹²⁹Xe | brown adipose tissue | thermometry | FDG-PET

Obesity is the result of an imbalance between energy intake and energy expenditure. The latter seems to be modulated, at least in part, by the activity of brown adipose tissue (BAT). BAT is a fatty tissue specialized in cold-induced and diet-induced thermogenesis, a metabolic activity during which this tissue burns fat to produce heat (1). Because of its high “fat-burning” capacity and its ability to regulate glucose homeostasis and insulin sensitivity (2, 3), this tissue is now considered to be the next target for antiobesity drugs (4). However, as interventions that aim to decrease body weight by increasing energy expenditure through BAT volume and/or activity modulations are being investigated (5, 6), the ability to detect this tissue in humans represents an unmet need. Current imaging techniques fail to detect BAT in the target population, obese and overweight subjects, and it is not clear whether this is due to a lack of BAT mass or BAT activity (7). For example, ¹⁸FluoroDeoxyGlucose Positron Emission Tomography (¹⁸FDG-PET), considered to be the gold standard for the detection of BAT activity, can detect BAT activity in morbidly obese and obese subjects only after bariatric surgery or substantial weight loss (8, 9). This is because ¹⁸FDG-PET can only be used to detect active BAT, and in obese subjects, activity is substantially reduced. In addition, the detection of BAT by ¹⁸FDG-PET is performed indirectly, through measurements of BAT uptake of glucose, which is not the primary fuel for BAT thermogenesis. Heat production in BAT is primarily fueled by oxidation of fatty acids released from triglycerides stored in the intracellular fat droplets (10), and, as such, measurements of exogenous glucose or exogenous fatty acid uptake are clearly intrinsically insensitive to BAT thermogenic activity (11, 12).

In computed tomography (CT) and ¹H MRI studies, fat fraction measurements are used to differentiate the highly hydrated brown adipose tissue from the less hydrated normal white adipose tissue (WAT) (13–15). Unfortunately, human BAT is a heterogeneous mixture of white and brown adipocytes (16), and partial volume effects that arise from the limited spatial resolution of these imaging modalities make these types of

measurements unreliable and nonspecific. Indeed, in one study in which ¹⁸FDG-PET BAT maps and MRI BAT maps were compared, areas that were BAT-positive for ¹⁸FDG-PET had the same fat fraction of nearby areas that were BAT-negative (17). Nonlinear MRI techniques based on intermolecular zero-quantum coherences between water and fat spins can be used to overcome partial volume effects and obtain background-free maps of BAT in lean phenotypes (18). However, in overweight and obese subjects, the strong reduction in tissue hydration and increase in the average distance between water and fat spins would cause a reduction of the already small nonlinear MR signal, making the entire detection unfeasible (18). More importantly, BAT hydration is not a good marker for BAT, as it is highly modulated by tissue thermogenic activity and therefore exhibits very high intersubject and intrasubject variability (19). For example, whereas in lean subjects BAT may have a fat fraction close to 50%, in obese subjects the BAT fat fraction is close to 80%, making it impossible to distinguish this tissue from the normal WAT with conventional fat fraction methods or more sophisticated nonlinear MR techniques.

Other less expensive imaging modalities such as infrared thermography and contrast ultrasound have similar problems. BAT thermogenesis is still detected indirectly, either through surface temperature measurements (infrared thermography) that are inherently affected by local changes in tissue blood flow (20) or by measurements of tissue blood flow (ultrasound), which is only partially coupled to BAT thermogenic activity (11) and which exhibits the same insensitivity to the less vascularized lipid-rich BAT of obese phenotypes (21).

Our primary goal with this study is to evaluate the possibility to detect BAT tissue and thermogenic activity by using hyperpolarized

Significance

In recent years, there has been a growing interest in brown adipose tissue (BAT), a tissue specialized in nonshivering thermogenesis and considered to be the next therapeutic target against obesity and diabetes. However, the detection of this very sparse tissue still represents a major challenge. To our knowledge, we report the first *in vivo* detection of BAT and thermogenic activity by hyperpolarized xenon gas MRI. We show that during thermogenic activity a more than 15-fold enhancement in xenon uptake by BAT enables us to clearly differentiate this tissue from the surrounding tissue and to thereby overcome the major limitations of conventional imaging methods. We also use lipid-dissolved hyperpolarized xenon chemical shift to demonstrate direct *in vivo* MR thermometry of BAT.

Author contributions: R.T.B. designed research; R.T.B., T.H., L.Z., M.F., C.W., and A.B. performed research; R.T.B., T.H., and C.S.F. analyzed data; and R.T.B. wrote the paper.

The authors declare no conflict of interest.

*This Direct Submission article had a prearranged editor.

¹To whom correspondence should be addressed. Email: rbranca@unc.edu.

This article contains supporting information online at www.pnas.org/lookup/suppl/doi:10.1073/pnas.1403697111/-DCSupplemental.

(HP) xenon gas MRI. In hyperpolarized xenon MRI studies, prior hyperpolarization of the gas through a process called spin-exchange optical pumping (SEOP) is the necessary step to make the gas MR-visible (22). After hyperpolarization, the gas can be inhaled by the subject or by the animal to visualize lung ventilation function (23), xenon gas exchange (23, 24), or other distal organs of interest (25). After inhalation the gas diffuses from the lung airspaces to the lung parenchyma and to the blood. The dissolved gas is then transported to distal organs, where it accumulates proportionally to tissue perfusion rate and to tissue–blood partition coefficient. More interestingly, as xenon diffuses in different tissue compartments, its chemical shift changes, making it possible to differentiate between xenon dissolved in blood and xenon dissolved in tissue or lipids. However, as the amount of xenon that is transferred at any given point in time from the lung airspaces to tissue–blood is relatively small, and as the T₁ relaxation time of xenon in blood is relatively short, imaging of distal organs by hyperpolarized xenon gas remains a major challenge.

Here we capitalize on the lipophilic nature of xenon and on the strong increase in blood flow to brown fat that occurs during stimulation of thermogenic activity to detect the highly vascularized BAT (26). In addition, we measure and use the chemical shift temperature coefficient of xenon dissolved in adipose tissue to directly detect its thermogenic activity *in vivo*.

Results

Spectroscopic Measurements of Xenon Dissolved in BAT. Fig. 1A and B shows stacked plots of representative dynamic ¹²⁹Xe spectra acquired on an anesthetized lean (C57BL6) (Fig. 1A) and on an obese (ob/ob) (Fig. 1B) mouse during ventilation with a mixture of oxygen and hyperpolarized xenon (26.4% of ¹²⁹Xe) gas in a 25/75 ratio. The spectra are acquired before and during stimulation of BAT thermogenesis, which is achieved by an i.p. injection of NorEpinephrine (NE), a catecholamine commonly used to stimulate BAT activity by mimicking the effect of cold exposure in anesthetized mice. Whereas before stimulation of BAT thermogenesis the predominant peak in both mouse strains is the gas-phase peak at 0 ppm, as expected, during stimulation of BAT thermogenesis a more than 15-fold enhancement of the dissolved-phase peaks is observed. More specifically, upon stimulation of BAT thermogenesis, two main dissolved-phase peaks become visible: the lipid-dissolved xenon peak at about 189 ppm and an additional peak at about 198 ppm, which is known to correspond to xenon dissolved in the intracellular water compartment (cell cytoplasm) (27). Interestingly, whereas in lean mice these two peaks are comparable in size (mean amplitude

ratio was about 2 ± 1), in obese mice the lipid-dissolved peak is by far the predominant peak (mean amplitude ratio was about 18 ± 8). This dichotomy observed between lean and obese mice seems to reflect the differences in BAT hydration and tissue blood perfusion between the two phenotypes. In lean mice, BAT is highly perfused and exhibits the characteristic multilocular structure: a large number of small lipid droplets surrounded by abundant cytoplasm (Fig. 1, *Inset*). As such, perfused xenon dissolves in the lipid compartment of the cell (lipid droplets) as well as in the intracellular water compartment in a manner that depends on the solubility of xenon in these two compartments (28). Conversely, in obese mice BAT is swollen with fat, and therefore the intracellular water compartments are considerably reduced, leading to a predominant accumulation of xenon in the fat droplets. Despite the reduced vascularization and increased fat content, BAT in these animals is still viable, as is demonstrated by the presence of UCP1 [a marker gene for brown adipose tissue whose presence is essential for the identification of a fat depot as BAT depot (1) in the BAT of the obese mouse].

Soon after inhalation of hyperpolarized (HP) xenon, blood transports xenon to BAT where xenon magnetization rapidly builds up. The xenon magnetization buildup curve in Fig. 2 shows that xenon magnetization in BAT reaches about 50% of its maximum value at about 4–5 s and a steady state after about 15–20 s.

Imaging of BAT by HP ¹²⁹Xe and Comparison with ¹⁸F-FDG-PET and Fat Fraction Measurements.

We confirm through imaging that the signal enhancement observed upon stimulation of BAT thermogenesis is due to a specific increase of xenon dissolved in BAT. Fig. 3 shows representative axial images of lean (Fig. 3A and B) and obese (Fig. 3C and D) mice before (Fig. 3A and C) and during (Fig. 3B and D) stimulation of BAT thermogenesis. Whereas before stimulation no appreciable signal is observed in the interscapular BAT (iBAT) region of these animals, a strong localized signal enhancement is observed during adrenergic stimulation of thermogenesis only in the area corresponding to iBAT. The local signal enhancement is also more than 10-fold, and from a simple signal to noise ratio (SNR) comparison with our ¹²⁹Xe-enriched thermally polarized phantom we estimated the local xenon concentration to be on the order of few micromolars, or more than two orders of magnitude larger than the maximum xenon concentration expected in the brain upon inhalation (29).

Fig. 3 also shows the higher sensitivity of hyperpolarized xenon gas MRI over positron emission tomography with [¹⁸F]-fluorodeoxyglucose (¹⁸FDG-PET) combined with computer tomography (CT) (Fig. 3E and F) and fat fraction MR measurements

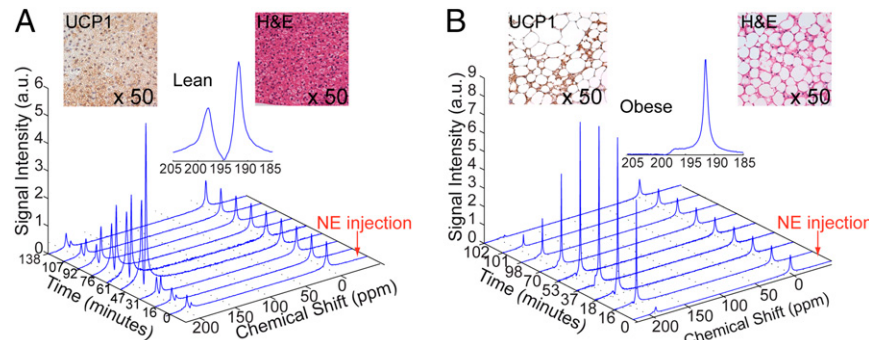


Fig. 1. Enhancement of xenon uptake in BAT upon stimulation of thermogenesis. Temporal dynamics of hyperpolarized ¹²⁹Xe resonances as acquired in a lean (A) and in an obese (B) animal before and during NE stimulated thermogenesis. All spectra are normalized to the gas-phase peak. (*Inset*) Hyperpolarized xenon spectra acquired after the injection of NE show two predominant peaks, one at 190 ppm corresponding to lipid-dissolved xenon and one at 198 ppm, corresponding to xenon dissolved in the cell cytoplasm. *Inset* also shows H&E-stained slides and UCP1 stained slides of BAT in the two mice. The H&E slides show larger lipid droplets (white) and a higher fat content in the obese mouse BAT. UCP1 stained slides of BAT show the presence of UCP1 (brown color) in both phenotypes, although UCP1 content is considerably reduced in the BAT of obese mice.

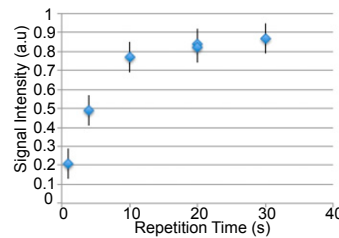


Fig. 2. Time-dependent accumulation of polarized ^{129}Xe in BAT. The measured lipid-dissolved xenon line amplitude was normalized to the gas-phase line amplitude. Measurements were done serially on one obese mouse, 4 min after Norepinephrine injection, using a single 300-mL Tedlar bag.

(Fig. 3 G and H) for the detection of the BAT of obese mice. Whereas in lean mice, glucose uptake by iBAT greatly exceeds that from surrounding tissues (Fig. 3F) and fat fraction is close to 50% (Fig. 3H), in obese mice, glucose uptake by iBAT is markedly reduced (Fig. 3E) and fat fraction is close to that of surrounding tissues (Fig. 3G), making it less useful in BAT identification and differentiation. On the other hand, HP xenon gas MRI can specifically detect this tissue in both strains without loss of sensitivity for the lipid-rich and less active BAT of obese mice.

Temperature Measurements by Hyperpolarized ^{129}Xe . We also investigate the possibility of using hyperpolarized xenon to directly measure BAT temperature during thermogenic activity. MR temperature measurements are based on the relatively weak temperature dependence of the water chemical shift ($-0.01\text{ ppm}/^\circ\text{C}$) (30). In fatty tissues these measurements are notoriously challenging, as the water resonance frequency is also affected by the temperature-dependent susceptibility gradients (31). Although the use of nonlinear MR techniques could partially circumvent this problem (32), the intrinsically low intensity of these nonlinear signals coupled with the strong reduction in T_2^* that occurs in BAT during stimulation of thermogenic activity (33) makes these types of measurements unfeasible.

Starting from previous *in vitro* studies that have shown a strong temperature dependence of the chemical shift of xenon dissolved in lipid-like compounds such as olive oil (34), we decided to investigate the temperature dependence of xenon dissolved in adipose tissue *in vivo*. Fig. 4B shows the resonance frequency of xenon dissolved in the abdominal white adipose tissue of an obese mouse as a function of body temperature. The graph shows a linear inverse relation between temperature and the resonance frequency of xenon dissolved in the tissue with a coefficient of $(-0.2 \pm 0.01)\text{ ppm}/^\circ\text{C}$, a factor of about 20 higher than the chemical shift temperature dependence of water protons ($-0.01\text{ ppm}/^\circ\text{C}$) currently used for MR thermometry in lean tissues.

BAT Temperature Measurements by Hyperpolarized ^{129}Xe . This higher temperature dependence allowed us to directly and accurately measure BAT temperature during thermogenic activity with a precision of $0.2\text{ }^\circ\text{C}$. Fig. 5 shows the results of dynamic spectroscopy studies conducted in lean and obese mice right after stimulation of thermogenesis, during which we tracked the resonance frequency of the lipid-dissolved xenon spins, animal rectal temperature, and bore temperature. The graph shows a rapid downshift of the lipid-dissolved xenon frequency right after the injection of NE. This downshift, consistent with the inverse relation found previously between lipid-dissolved xenon frequency and temperature, corresponds to an increase in BAT cell temperature, which, in both strains, rose for about 20–30 min before declining again, a trend similar to that found outside the magnet using BAT temperature probes (Fig. 5C). Interestingly,

whereas in all four normal lean mice, analyzed BAT temperature rose on average by $6 \pm 2\text{ }^\circ\text{C}$, in the three obese mice, analyzed BAT temperature rose on average by $2 \pm 1.5\text{ }^\circ\text{C}$, confirming that in this strain, BAT is not only relatively atrophied and swollen with fat but is also partially thermogenetically quiescent (35, 36), as is also indicated by the reduced expression of UCP1 (Fig. 1, *Inset*). Nonetheless, despite the diminished thermogenic capacity in this strain, we were able to obtain clear maps of this tissue.

Discussion and Conclusions

In this paper we demonstrated detection of BAT tissue and thermogenic activity by hyperpolarized xenon gas MRI. Despite the known challenges associated with HP xenon MR detection of peripheral organs, several factors contribute to the successful detection of this tissue. First, with about $1,000$ capillary/mm 2 (21), BAT has a capillary density similar to that of skeletal muscle. In addition, during stimulation of BAT thermogenic activity by either NE injection or by cold exposure, blood flow to BAT is known to increase by more than 15-fold (21, 37) in response to the increased oxygen demand of this tissue. These two factors coupled with the high solubility of xenon in fat [which is more than 10 times higher than in blood and lean tissue (38)] are the key elements that lead to the observed 15-fold enhancement

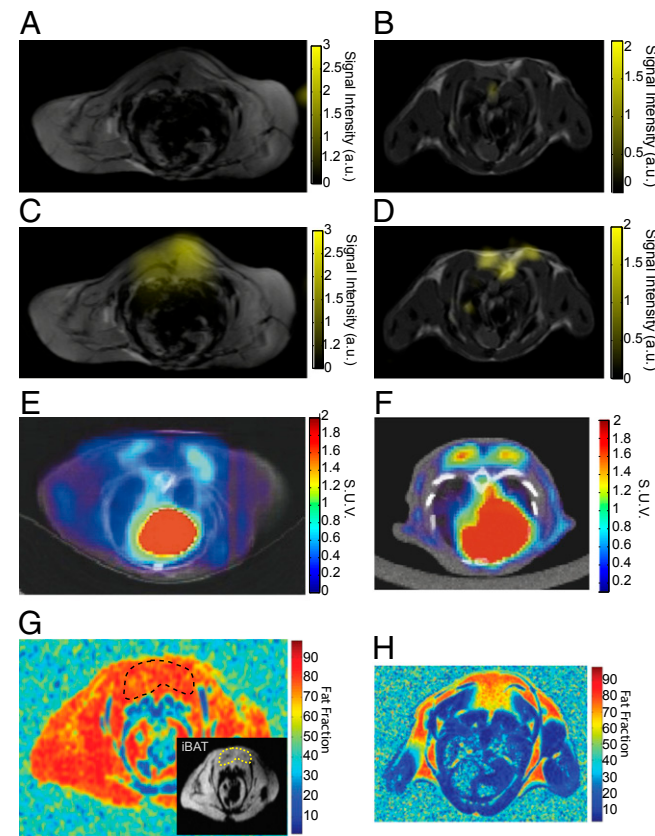


Fig. 3. HP ^{129}Xe maps of interscapular BAT in lean and obese mice and comparison with ^{18}F -FDG-PET/CT. The figure shows the detection of BAT by HP ^{129}Xe MRI, ^{18}F -FDG-PET, and fat fraction 1H MRI in lean (Right) and in obese (Left) mice. Hyperpolarized dissolved-phase xenon images are displayed as a false color overlay on the corresponding 1-mm-thick axial proton reference image at baseline (A and B) and during stimulation of BAT thermogenesis (C and D) in the same animals. (E and F) The ^{18}F -FDG-PET/CT images in a lean (F) and obese (E) animal during stimulation of BAT thermogenesis. (G and H) Fat fraction 1H MR measurements in a lean (H) and obese (G) mouse. Inset in G delineates the interscapular BAT in the obese mouse.

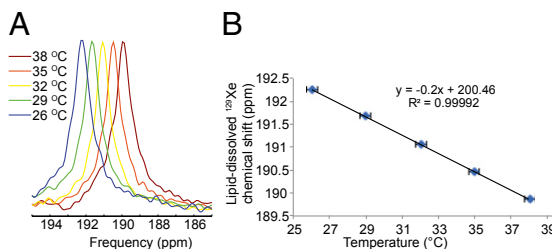


Fig. 4. Lipid-dissolved ¹²⁹Xe frequency as a function of temperature as acquired from the abdomen of an obese mouse acclimated at different bore temperatures. (A) Experimental frequency shift of the lipid-dissolved peak. (B) Resonance frequency of the lipid-dissolved peak as function of body temperature. A clear linear temperature dependence of the lipid-dissolved xenon resonance frequency can be observed in the 26–37 °C temperature range analyzed.

of xenon signal from BAT. The enhancement is very localized and large enough to enable the fast acquisition of background-free maps of this tissue, with relatively low polarization levels (8–10%) and without the use of more expensive ¹²⁹Xe-enriched gas.

Interestingly, xenon signal enhancement is observed not only in lean but also in the obese mouse phenotype in which capillary density, tissue blood flow, and thermogenic activity are all known to be reduced (21). This is probably because the lipid-rich BAT of obese mice represents a better host for lipophilic xenon, thereby compensating for the reduction in blood flow and capillary density. In our opinion, the ability to detect this tissue in both lean and obese phenotypes represents one of the major advantages over existing methodologies, none of which can be used to detect BAT and its activity in obese and overweight subjects, the target population for antiobesity treatments that are tailored to activating BAT. Despite our belief that all humans possess brown adipose tissue, all measurements performed in humans seem to indicate that overweight subjects and obese subjects lack BAT activity (¹⁸F-FDG-PET) and BAT mass (MRI) (7, 13). Clearly, in obese subjects, BAT fat content is similar to that of normal WAT, precluding its visibility from MR fat fraction measurements. Similarly, because of its high intracellular fatty acid loading and intrinsically low thermogenic activity, lipid-rich BAT, even if fully stimulated, will rely less on circulating sources of energy to sustain thermogenesis, making its ¹⁸F-FDG-PET detection challenging (11, 12). This is indeed what has been hypothesized (11) and what we have also shown here with mouse studies. Conversely, hyperpolarized ¹²⁹Xe MRI can clearly be used to identify this tissue, regardless of its hydration status and even if thermogenic activity, blood flow, and capillary density are substantially diminished.

Xenon spectra allow us to also quantify mean tissue hydration associated with average and acute thermogenic activity. Information on mean tissue hydration can be obtained from the relative ratio of the two dissolved-phase peaks after proper peak normalization. Peak normalization is needed to account for the different solubility and for the different T1 and T2* relaxation time of xenon in the two compartments. Once mean tissue hydration has been obtained, this measurement coupled with 3D volume maps of BAT could be used to directly quantify BAT mass. In mice the acquisition of 3D maps should be relatively straightforward with the use of enriched xenon, which will boost the SNR by a factor of three. In humans the acquisition of 3D maps may be challenging, considering the longer time xenon spends in the blood in its journey from the lung airspaces to BAT tissue (39, 40) and the reduced increase in tissue blood flow (41). However, the lipophilic nature of xenon and the high vascularization of brown adipose tissue should still lead to an in-tissue concentration on the order of a few tens of micromoles, which

should allow the acquisition of xenon spectra (42) from which tissue hydration and thermogenic activity could be inferred. In addition, because in humans the resonance frequency of xenon dissolved in red blood cells is well resolved from that of xenon in tissue, information on the concurrent increase in tissue blood flow (43), and perhaps blood oxygenation, could be obtained.

The other major advantage of this technique is its ability to directly measure BAT temperature and to monitor its thermogenic activity in real time. We demonstrated that the chemical shift temperature coefficient of xenon dissolved in lipids is 20-fold higher than the chemical shift temperature coefficient of water protons commonly used for MR thermometry of lean tissues. This higher temperature dependence, coupled with the intrinsically lower sensitivity of the ¹²⁹Xe nucleus to magnetic field susceptibility gradients, allowed us to make BAT temperature measurements with a precision of 0.2 °C. Although these are all relative temperature measurements, we envision the possibility to also measure absolute temperature of fatty tissues. The almost temperature-insensitive resonance frequency of lipid protons could indeed be used as a reference for the temperature-sensitive lipid-dissolved xenon spins to extract absolute temperature information. Although the increase in BAT temperature in humans seems to be of lower magnitude, the high sensitivity of the lipid-dissolved xenon chemical shift to temperature should easily enable the detection of these smaller BAT temperature changes (<1 °C).

In conclusion, we demonstrate with this study the detection of BAT and thermogenic activity in lean and obese mice by hyperpolarized xenon gas MRI. As there is an increased interest in pharmacological interventions to stimulate BAT, measurements of BAT mass and thermogenesis by hyperpolarized xenon gas could become an important tool for understanding the role of this tissue in human metabolism and energy balance, for monitoring response to treatments, and to finally answer the question of whether obese subjects lack BAT activity or BAT mass altogether.

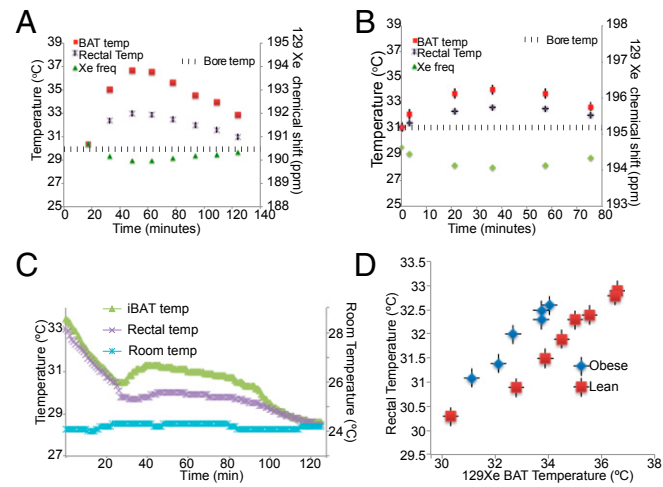


Fig. 5. Detection of BAT thermogenic activity. BAT temperature as a function of time after stimulation of BAT thermogenesis in a lean (A) and in an obese (B) animal as measured by the frequency shift of the lipid-dissolved xenon peak. The graph also shows the corresponding increase in BAT rectal temperature as detected by an MR-compatible rectal probe. Similar temperature behavior is seen using temperature probes inserted below the BAT in a lean phenotype (C). (D) BAT temperature, as measured by the lipid-dissolved xenon resonance frequency shift, as a function of mouse rectal temperature. BAT temperature does not correlate well with rectal temperature; during thermogenic activity it is expected to be higher than rectal temperature.

Methods

Animal Preparation. All animal studies were conducted under an animal protocol approved by the Institutional Animal Care and Use Committee at the University of North Carolina at Chapel Hill. A total of 17 obese (ob/ob) mice and 13 lean (C57BL6) mice, between 8 and 12 wk of age, were used in this study. Before the experiments, mice were first anesthetized with an i.p. injection of 60 mg/kg of pentobarbital (Nembutal, Abbott Laboratories). For the MR imaging and spectroscopy of hyperpolarized xenon studies, mice were intubated using a 22-gauge catheter (Sherwood Medical) and ventilated at a rate of 60 breaths per minute with a tidal volume of ~0.20 mL. During ^{129}Xe imaging, breathing gas was switched from air to a mixture of 75-vol% of HP ^{129}Xe (isotopic abundance) and 25-vol% of O_2 to achieve a tidal volume of 0.20 mL. The ventilator triggered the MRI scanner at the beginning of each breath hold. Airway pressure and ECG were monitored continuously. Anesthesia was maintained with periodic injection (about every 40 min) of pentobarbital at 1/4 of the initial dose. Bore temperature was measured and maintained using a closed loop temperature control system that included warm air circulating through the bore and a fiber optic temperature probe used to monitor bore temperature, which resulted in a temperature variation inside the bore of less than 0.1 °C (Small Animal Instruments). Rectal temperature was monitored by using an MR-compatible rectal probe. During MR examination, BAT thermogenesis was stimulated by an i.p. injection of norepinephrine (Levophed, Hospira) in a dose of 1 mg/kg. All animals were killed at the end of the imaging study by an overdose of pentobarbital (250 mg/kg).

Hyperpolarization of ^{129}Xe . Xenon, with a natural abundance of ^{129}Xe (26%) (Linde Industrial Gas), was polarized by spin-exchange optical pumping using a commercial xenon polarizer (Polarean). The gas was polarized using continuous flow and cryogenic extraction in about 20 min. The gas was collected in a 300- or 150-mL Tedlar bag (Jensen Inert Products), housed inside a Plexiglas cylinder, and used after less than 1 min to collect imaging or spectroscopy data. A hose connected the cylinder to a homemade constant-volume HP gas-compatible ventilator. Xenon gas polarization was measured to be between 8.5% and 10%.

Magnetic resonance imaging and spectroscopy of BAT. All MR imaging and spectroscopy experiments were performed on a 9.4T Bruker Biospec Avance MRI system controlled by a console running ParaVision software. A surface xenon coil (1-cm diameter, transmit and receive, 110.76 MHz) was positioned either above the interscapular BAT depot to acquire spectroscopy and imaging ^{129}Xe data on interscapular BAT or above the lower abdomen of the mouse to acquire the temperature-dependent chemical shift curves. The surface coil was placed inside a ^1H volume coil (72-mm inner diameter, transmit and receive, 400 MHz) to enable the acquisition of high-resolution anatomical reference images. These images were acquired with a gradient echo sequence using the following parameters: an echo time (TE) of 5 ms, a repetition time (TR) of 3,000 ms, a matrix size (MTX) of 128 × 128, a Field of View (FOV) of 55 mm, and a slice thickness of 1 mm.

HP ^{129}Xe images of BAT were acquired on three lean and three obese mice with a gradient echo sequence using the following parameters: 90° adiabatic excitation pulse [1 ms duration, B1-insensitive rotation (BIR-4)], TE = 2 ms, TR = 4 s, NA (number of averages) = 2, FOV = 55 × 55 mm², and MTX = 32 × 32. A spectral width (SW) of 50 kHz (~14 ppm/pixel) allowed us to completely separate the dissolved-phase image from the gas-phase image (Fig. S1). For both imaging and spectroscopy data, a repetition time of 4 s was chosen as a compromise to decrease scan time and allow sufficient accumulation of xenon in tissue. Image acquisition started less than 1 min after xenon thawing and lasted for about 4 min. Images were not corrected for xenon depolarization inside the bag and were interpolated using Matlab to increase the spatial resolution from 1.7 × 1.7 mm² to 0.85 × 0.85 mm² (Fig. S1 C and D).

HP ^{129}Xe spectra were acquired on two lean and two obese mice using a pulse flip angle of 90° (1 ms duration, adiabatic BIR-4 pulse), TR = 4 s, NA = 20, SW = 501.57 ppm, and a number of points (Npoints) of 2,048. Each FID raw data set was zero-filled to 4,096 points and Fourier-transformed without apodization. The spectrum was then baseline-corrected and normalized to the gas-phase peak. Correction for T1 relaxation inside the Tedlar bag was not performed. Each spectrum was acquired using a single bag of 150 mL hyperpolarized xenon. Total acquisition time for each spectrum was about 80 s.

Fat fraction measurements were performed on one lean and one obese animal using frequency-selective water and fat spin-echo sequences (TE/TR = 15 ms/6 s, FOV = 55 × 55 mm², MTX = 256 × 256, and slice thickness = 1 mm) preceded by a saturation module (selective excitation by a 600-Hz Gaussian pulse followed by crush gradients along all three directions). Specifically, water images were acquired using a fat saturation suppression module followed by a water-selective spin-echo sequence. Similarly, fat images were

acquired by using a water suppression saturation module followed by a fat-selective spin-echo sequence. Fat fraction images were then obtained using homemade Matlab code that performed a pixel-by-pixel calculation of fat fraction [$\text{SI}_{\text{fat}}/(\text{SI}_{\text{fat}} + \text{SI}_{\text{water}})$], where SI_{fat} represents the fat image signal intensity and SI_{water} represents the water image signal intensity.

The xenon curve was obtained from one ob/ob mouse by serially acquiring spectra with different repetition times: TR = 1, 4, 10, 20, and 30 s. The acquisition of these spectra occurred about 3 min after norepinephrine injection by using a single 300-mL bag of polarized ^{129}Xe gas. Spectra were all acquired using a BIR-4 excitation pulse (90° flip angle and 1 ms duration), NA = 4 (TR = 1, 4, 10, and 20 s) or NA = 2 (TR = 20 and 30 s), SW = 501.57 ppm, and Npoints = 2,048. Each acquisition was followed by a crush module (90 degree, 1 ms, BIR-4 pulse surrounded by crush gradients of different strengths and durations). Each FID raw data set was zero-filled to 4,096 points and Fourier-transformed without apodization. The spectrum was then baseline-corrected, and the dissolved-phase signal intensity was then normalized to the gas-phase peak, to account for variation in xenon polarization due to T1 relaxation inside the Tedlar bag.

Temperature coefficient study. For the calibration of the temperature coefficient of the lipid-dissolved xenon chemical shift we ran a series of non-localized spectra on four obese mice with the xenon surface coil-positioned above the abdominal white fat depot. An MR-compatible rectal probe was used to control mouse body temperature. Bore temperature was varied between 37 °C and 26 °C and controlled to ±0.1 °C. Before the acquisition of each data point the animal was acclimated to the new temperature for at least 30 min.

The lipid-dissolved xenon resonance frequency was measured using the same protocol and spectroscopy parameters used for the acquisition of the BAT spectra except for the repetition time, which was set to TR = 20 s and NA = 4. The FID data were zero-filled to 4,096 points and Fourier-transformed without apodization. After baseline correction, the resonance frequency of the lipid-dissolved xenon peak was found by fitting the spectrum with a Voigt function, using a homemade Matlab code. Because the lungs were outside the sensitive region of the surface coil, no gas-phase peak was detected, and the chemical shift value of lipid-dissolved xenon was arbitrarily set around 190 ppm.

For the acquisition of BAT temperature curves using the lipid-dissolved xenon chemical shift, an MR-compatible rectal probe was used to control mouse rectal temperature. Bore temperature was set and maintained at 29.5 °C or 30 °C with an accuracy of ±0.1 °C for lean and obese mice, respectively. Before norepinephrine injection, the animal was acclimated to the set bore temperature at least for 30 min. The ^{129}Xe spectra were acquired using the exact same procedure used to acquire the dynamic spectroscopy data, with TR = 4 s and NA = 20. The FID data were zero-filled to 4,096 points and Fourier-transformed without apodization. After baseline correction, the resonance frequency of the lipid-dissolved xenon peak was found by fitting the spectrum with Voigt functions, using a homemade Matlab code. The resonance frequency of the lipid-dissolved peak was then transformed into BAT temperature by using the -0.2 ppm/°C temperature coefficient found previously.

$^{18}\text{FDG-PET/CT imaging of BAT}$. The $^{18}\text{FDG-PET/CT}$ scans were performed using the GE eXplore Vista small animal PET/CT system. For the PET studies, four lean and four ob/ob mice at 12 wk of age were used. All animals were first anesthetized with pentobarbital (60 mg/kg) and then kept under anesthesia by periodic injections of pentobarbital (1/4 initial dose every 40 min). The anesthetized animal then received an i.p. injection of norepinephrine (1 mg/kg) 5 min before the injection of the radiotracer (200 microcuries in 0.2 mL). PET/CT scans started 5 min after ^{18}F -FDG injection. Images were acquired with an intrinsic spatial resolution of 2 mm and reconstructed using a filtered back-projection algorithm without scatter or attenuation correction.

Histology. After imaging, mice were killed with an overdose of pentobarbital (250 mg/kg). An incision was made above the interscapular brown fat depot, which was then excised. The tissue was fixed in formalin for 24 h, embedded in paraffin and serially sectioned to 5 μm, mounted onto adhesive slides, and finally stained with H&E. This staining, in which lipid droplets appear as a small or large empty vacuoles within the pink cell's cytoplasm, was used to visually assess the degree of BAT hydration in the different mouse strains.

For UCP1 immunohistochemistry staining, which produces a brown stain in presence of UCP1, the sections were dewaxed and rehydrated in a series of graded alcohols. Heat-induced epitope retrieval was performed in citrate buffer (pH 6.0) in a steamer for 20 min. The blocking procedure was carried out using Cyto-Q Background Buster (Innovex; NB306) for 30 min followed by UCP1 primary antibody incubation for 1 h at room temperature (1:250; ab10983; Abcam). Secondary antibody incubation and detection were performed for 30 min with biotinylated goat anti-rabbit (1:200; BA100; Vector) and VectrStain Elite ABC complex, respectively (Vector). The slides were then incubated in diaminobenzidine and counterstained in hematoxylin.

To examine the typical BAT thermogenic response to norepinephrine, BAT temperature, rectal temperature, and room temperature were all monitored before and after NE injection outside the magnet using temperature probes in four C57BL/6 mice and three ob/ob mice. To monitor BAT temperature, a temperature probe was surgically inserted below the interscapular BAT pad and sutured into place. A temperature probe was inserted 1 cm into the rectum to

monitor rectal temperature, and a third temperature probe was placed 2 cm away from the animal to monitor room temperature.

ACKNOWLEDGMENTS. This work was largely supported by the National Institute of Diabetes and Digestive and Kidney Diseases (Grant R21 DK090758) and partially supported by the National Cancer Institute (R01-CA142842).

1. Cannon B, Nedergaard J (2004) Brown adipose tissue: Function and physiological significance. *Physiol Rev* 84(1):277–359.
2. Rothwell NJ, Stock MJ (1983) Luxuskonsumption, diet-induced thermogenesis and brown fat: The case in favour. *Clin Sci (Lond)* 64(1):19–23.
3. Stanford KI, et al. (2013) Brown adipose tissue regulates glucose homeostasis and insulin sensitivity. *J Clin Invest* 123(1):215–223.
4. Nedergaard J, Cannon B (2010) The changed metabolic world with human brown adipose tissue: Therapeutic visions. *Cell Metab* 11(4):268–272.
5. Cypress AM, et al. (2009) Identification and importance of brown adipose tissue in adult humans. *N Engl J Med* 360(15):1509–1517.
6. Yoneshiro T, et al. (2013) Recruited brown adipose tissue as an antiobesity agent in humans. *J Clin Invest* 123(8):3404–3408.
7. van Marken Lichtenbelt WD, et al. (2009) Cold-activated brown adipose tissue in healthy men. *N Engl J Med* 360(15):1500–1508.
8. Vijgen GHEJ, et al. (2012) Increase in brown adipose tissue activity after weight loss in morbidly obese subjects. *J Clin Endocrinol Metab* 97(7):E1229–E1233.
9. Vijgen GHEJ, et al. (2011) Brown adipose tissue in morbidly obese subjects. *PLoS ONE* 6(2):e17247.
10. Ma SW, Foster DO (1986) Uptake of glucose and release of fatty acids and glycerol by rat brown adipose tissue in vivo. *Can J Physiol Pharmacol* 64(5):609–614.
11. Cannon B, Nedergaard J (2012) Yes, even human brown fat is on fire! *J Clin Invest* 122(2):486–489.
12. Ouellet V, et al. (2012) Brown adipose tissue oxidative metabolism contributes to energy expenditure during acute cold exposure in humans. *J Clin Invest* 122(2):545–552.
13. Saito M, et al. (2009) High incidence of metabolically active brown adipose tissue in healthy adult humans: Effects of cold exposure and adiposity. *Diabetes* 58(7):1526–1531.
14. Hu HH, Tovar JP, Pavlova Z, Smith ML, Gilsanz V (2012) Unequivocal identification of brown adipose tissue in a human infant. *J Magn Reson Imaging* 35(4):938–942.
15. Baba S, Jacene HA, Engles JM, Honda H, Wahl RL (2010) CT Hounsfield units of brown adipose tissue increase with activation: Preclinical and clinical studies. *J Nucl Med* 51(2):246–250.
16. Virtanen KA, et al. (2009) Functional brown adipose tissue in healthy adults. *N Engl J Med* 360(15):1518–1525.
17. van Rooijen BD, et al. (2013) Imaging cold-activated brown adipose tissue using dynamic T2*-weighted magnetic resonance imaging and 2-Deoxy-2-[18F]fluoro-D-glucose positron emission tomography. *Investigat Radiol* 48(10):708–714.
18. Branca RT, et al. (2013) In vivo noninvasive detection of brown adipose tissue through intermolecular zero-quantum MRI. *PLoS ONE* 8(9):e74206.
19. Heaton JM (1972) The distribution of brown adipose tissue in the human. *J Anat* 112(Pt 1):35–39.
20. Lee P, et al. (2011) Hot fat in a cool man: Infrared thermography and brown adipose tissue. *Diabetes Obes Metab* 13(1):92–93.
21. Clerete M, et al. (2013) Brown adipose tissue blood flow and mass in obesity: A contrast ultrasound study in mice. *J Am Soc Echocardiogr* 26(12):1465–1473.
22. Albert MS, et al. (1994) Biological magnetic resonance imaging using laser-polarized ¹²⁹Xe. *Nature* 370(6486):199–201.
23. Mugler JP, 3rd, et al. (2010) Simultaneous magnetic resonance imaging of ventilation distribution and gas uptake in the human lung using hyperpolarized xenon-129. *Proc Natl Acad Sci USA* 107(50):21707–21712.
24. Driehuys B, Möller HE, Cleveland ZI, Pollaro J, Hedlund LW (2009) Pulmonary perfusion and xenon gas exchange in rats: MR imaging with intravenous injection of hyperpolarized ¹²⁹Xe. *Radiology* 252(2):386–393.
25. Mazzanti ML, et al. (2011) Distribution of hyperpolarized xenon in the brain following sensory stimulation: Preliminary MRI findings. *PLoS ONE* 6(7):e21607.
26. Foster DO (1984) Quantitative contribution of brown adipose tissue thermogenesis to overall metabolism. *Can J Biochem Cell Biol* 62(7):618–622.
27. Boutin C, et al. (2011) Hyperpolarized ¹²⁹Xe NMR signature of living biological cells. *NMR Biomed* 24(10):1264–1269.
28. Peled S, et al. (1996) Determinants of tissue delivery for ¹²⁹Xe magnetic resonance in humans. *Magn Reson Med* 36(3):340–344.
29. Martin CC, et al. (1997) The pharmacokinetics of hyperpolarized xenon: Implications for cerebral MRI. *J Magn Reson Imaging* 7(5):848–854.
30. De Poorter J, et al. (1995) Noninvasive MRI thermometry with the proton resonance frequency (PRF) method: In vivo results in human muscle. *Magn Reson Med* 33(1):74–81.
31. De Poorter J (1995) Noninvasive MRI thermometry with the proton resonance frequency method: Study of susceptibility effects. *Magn Reson Med* 34(3):359–367.
32. Galiana G, Branca RT, Jenista ER, Warren WS (2008) Accurate temperature imaging based on intermolecular coherences in magnetic resonance. *Science* 322(5900):421–424.
33. Khanna A, Branca RT (2012) Detecting brown adipose tissue activity with BOLD MRI in mice. *Magn Reson Med* 68(4):1285–1290.
34. Miller KW, et al. (1981) Xenon NMR: Chemical shifts of a general anesthetic in common solvents, proteins, and membranes. *Proc Natl Acad Sci USA* 78(8):4946–4949.
35. Himms-Hagen J, Desautels M (1978) A mitochondrial defect in brown adipose tissue of the obese (ob/ob) mouse: Reduced binding of purine nucleotides and a failure to respond to cold by an increase in binding. *Biochem Biophys Res Commun* 83(2):628–634.
36. Cannon B, Nedergaard J (1985) The biochemistry of an inefficient tissue: Brown adipose tissue. *Essays Biochem* 20:110–164.
37. Foster DO, Frydman ML (1978) Nonshivering thermogenesis in the rat. II. Measurements of blood flow with microspheres point to brown adipose tissue as the dominant site of the calorigenesis induced by noradrenaline. *Can J Physiol Pharmacol* 56(1):110–122.
38. Steward A, Allott PR, Cowles AL, Mapleson WW (1973) Solubility coefficients for inhaled anaesthetics for water, oil and biological media. *Br J Anaesth* 45(3):282–293.
39. Janssen B, Debets J, Leenders P, Smits J (2002) Chronic measurement of cardiac output in conscious mice. *Am J Physiol Regul Integr Comp Physiol* 282(3):R928–R935.
40. Thomasson B (1957) Cardiac output in normal subjects under standard basal conditions; the repeatability of measurements by the Fick method. *Scand J Clin Lab Invest* 9(4):365–376.
41. Müzik O, et al. (2013) ¹⁵O PET measurement of blood flow and oxygen consumption in cold-activated human brown fat. *J Nucl Med* 54(4):523–531.
42. Kilian W, Seifert F, Rinneberg H (2004) Dynamic NMR spectroscopy of hyperpolarized (¹²⁹Xe) in human brain analyzed by an uptake model. *Magn Reson Med* 51(4):843–847.
43. Mugler JP, 3rd, et al. (1997) MR imaging and spectroscopy using hyperpolarized ¹²⁹Xe gas: Preliminary human results. *Magn Reson Med* 37(6):809–815.